

# Inferring Neutron Star Properties via r-mode Gravitational Wave Signals

Dhanvarsh Annamalai\* and Rana Nandi†

*Department of Physics, School of Natural Sciences,*

*Shiv Nadar Institution of Eminence, Greater Noida 201314, Uttar Pradesh, India*

(Dated: June 21, 2024)

We present two frameworks to infer some of the properties of neutron stars from their electromagnetic radiation and the emission of continuous gravitational waves due to r-mode oscillations. In the first framework, assuming a distance measurement via electromagnetic observations, we infer three neutron star properties: the moment of inertia, a parameter related to the r-mode saturation amplitude, and the component of magnetic dipole moment perpendicular to the rotation axis. Unlike signals from mountains, r-mode oscillations provide additional information through a parameter ( $\kappa$ ) that satisfies a universal relation with the star's compactness. In the second framework, we utilize this and the relation between the moment of inertia and compactness, in addition to assuming an equation of state and utilizing pulsar frequency measurements, to directly measure the neutron star's distance along with the aforementioned parameters. We employ a Fisher information matrix-based approach for quantitative error estimation in both frameworks. We find that the error in the distance measurement dominates the errors in the first framework for any reasonable observation time. In contrast, due to the low errors in pulsar frequency measurements, parameters can be inferred accurately via the second framework but work only in a restricted parameter space. We finally address potential ways to overcome critical drawbacks of our analyses and discuss directions for future work.

---

\* dhanvarshannamalai2002@gmail.com

† rana.nandi@snu.edu.in

## I. INTRODUCTION

The new age of gravitational wave astronomy has the potential to provide more information than traditional astronomy or complement it in a useful way. Ever since the first detection of gravitational waves from a binary black hole merger event, GW150914, in 2015 [1], a plethora of compact binary inspirals has been detected ([2–4]). These detections have given us vital astrophysical insights such as confirming the existence of stellar-mass black holes and providing an association between binary neutron star mergers, gamma-ray bursts, kilonovae, and the production of heavy elements in the universe [5], constraining the equation of state high-density nuclear matter [6–8], etc.

Continuous gravitational waves (CGW), as yet an undiscovered type of gravitational wave, are weak pseudo-monochromatic signals that last over long time scales, produced by tiny mountains or velocity perturbations in the star. An important potential source for CGW is r-mode oscillations in neutron stars. These are quasi-normal modes driven unstable by gravitational radiation via the CFS instability ([9, 10]) with a frequency approximately equal to 4/3rd of the rotation frequency of the star. While we expect the modes to grow due to the instability [11] and eventually saturate because of damping, there are still uncertainties associated with the amplitude achievable by r-modes because of the non-linear hydrodynamics related to the damping mechanisms that limit the growth of the modes ([12–14]). We expect that the saturation phase will last a long time, consequently generating CGW.

Although CGW signals have not been detected yet, the prospects for future detection continue to improve with the increase in sensitivity of the upcoming detectors and the refinement of the data analysis techniques [15]. Current CGW searches have only set upper limits on the saturation amplitude  $\alpha_s$ , a parameter that characterises r-modes during the saturation phase, from all-sky [16], directed [17] and narrow-band searches ([18, 19]).

As the prospects of detection improve, it becomes important to address what can be learnt from such a detection. Under the assumption that a pulsar spins down just due to CGW, a recent study [20] showed that one can only infer the ratio of a macroscopic parameter (e.g. moment of Inertia, ellipticity) and the distance to the star. Thereafter, another study [21], explored inferring the properties of the star assuming the existence of an electromagnetic distance measurement, and, that the star spins down due to a dipolar magnetic field and CGW. They also assumed that the detected signals are produced by mountains in the

neutron star. This can be known with certainty, only in the case of targeted searches (when the rotation frequency of the star is known)[22]. The potential source could also be r-modes or other exotic possibilities [23, 24] for candidates detected via directed or all-sky searches. It has also been shown by [25] that one can directly measure the distance to the neutron star for signals produced by r-modes when the rotation frequency of the star is known. Based on these works, we investigate the parameter inference of a detected CGW signal produced by r-modes. In particular, we explore two different inference frameworks, assuming that the star spins down due to a dipolar magnetic field and CGW. In the first framework, similar to [21], we assume the existence of an electromagnetic distance measurement to the star post which we infer three neutron star properties: its moment of inertia ( $I$ ), the component of magnetic dipole moment perpendicular to the rotation axis ( $m_p$ ) and a parameter alpha ( $\alpha$ ) which is related to the saturation amplitude (Check Section II). In the second framework, we explore the case of signals detected particularly via narrow-band searches, where the distance to the star can be directly measured from the CGW signal along with the other macroscopic properties mentioned before.

This paper is organised as follows. Section II introduces the basics of CGW and their detection. Section III provides the two different theoretical frameworks used to infer neutron star properties. In Section IV, we discuss the Monte Carlo simulation used to present an error estimation study on the inferred parameters for both frameworks. Section V presents the results of these simulations. Section VI provides a summary of the work, and discusses key assumptions in this work, some drawbacks and potential ways to overcome them.

## II. PRELIMINARIES

In this section, we present the preliminary information relevant to this work. We introduce the signal model of a continuous gravitational wave (CGW) in section II A and the parameter estimation of the phase and amplitude parameters in section II B.

### A. Continuous Gravitational Wave Signal Model

During the saturation phase, the r-mode oscillations produce a continuous gravitational wave (CGW) signal dominated by  $l = m = 2$  current quadrupole [11]. In this period, the

noise-free strain  $h(t)$  in the detector is of the form [26]:

$$h(t) = \sum_{i=1}^4 \mathcal{A}_i h_i(t, \vec{\lambda}), \quad (1)$$

where  $\mathcal{A}_i$  are functions of the amplitude parameters: the characteristic strain amplitude ( $h_0$ ), the inclination angle ( $\iota$ ) between the Neutron star's rotation axis and line of sight, the polarization ( $\psi$ ) and initial phase ( $\phi_0$ ). The parameters represented by  $\vec{\lambda}$  are called the phase parameters; they include the star's sky position, the gravitational wave frequency ( $f$ ), the frequency derivatives ( $f^k$ ), and if the star is in a binary system, its orbital parameters. The signal model is similar to the one produced by mountains, except the polarization  $\psi$  must be reinterpreted as  $\psi + \frac{\pi}{4}$  for a signal produced by the r-mode oscillations [27].

The characteristic strain amplitude for r-mode oscillations is given by [27]:

$$h_0 = \sqrt{\frac{512\pi^7}{5}} \frac{G}{rc^5} f^3 \alpha_s M R^3 \tilde{J}, \quad (2)$$

where  $r$  is the distance to the star from SSB,  $M$  is the mass of the star,  $R$  is the radius of the star,  $\alpha_s$  is the r-mode saturation amplitude,  $f$  is the gravitational frequency which is approximately related to the rotational frequency of the neutron star by  $f \approx \frac{4}{3} f_{rot}$ , with corrections depending on the nuclear equation of state of the star [28], and  $\tilde{J}$  is a dimensionless parameter that also depends on the equation of state of the star and is given by [11]:

$$\tilde{J} = \frac{1}{MR^4} \int_0^R \varepsilon(r) r^6 dr, \quad (3)$$

where  $\varepsilon(r)$  is the energy density inside the neutron star.

Various mechanisms including gravitational waves and electromagnetic radiation could cause a Neutron star to spin down. Since the timescale of the observation of continuous gravitational waves is much less than the intrinsic timescale of the spin-down of the star, we can model the spin-down as a Taylor series [26]. Therefore, we model the evolution of the phase of the gravitational wave as a second-order Taylor series [29] (here  $\dot{f}, \ddot{f} \equiv f^1, f^2$ ):

$$\phi(t) = \phi_0 + 2\pi \left[ ft + \frac{1}{2} \dot{f} t^2 + \frac{1}{6} \ddot{f} t^3 \right]. \quad (4)$$

In Eq.(4), we have ignored the detector motion w.r.t the solar system barycenter (SSB), which is a satisfactory assumption when the star's sky position is known [29], which is the case in this work. An important parameter that is relevant in the study of the spin-down of

the star is the breaking index  $n$  given by:

$$n = \frac{f\ddot{f}}{\dot{f}^2}. \quad (5)$$

The value of  $n$  contains information regarding the spin-down mechanism of the neutron star [15]. If the star is just spinning down due to a current quadrupole moment produced by the r-modes, then  $n = 7$ . If it is spinning down purely due to a dipolar magnetic field, then  $n = 3$ . If the neutron star is spinning down just due to a mass quadrupole moment (mountains in the star), then  $n = 5$ .

## B. Gravitational Wave Parameter Estimation

Assuming that a true CGW signal is not appreciably different from the signal model in section II A, we expect to estimate the  $(h_0, f, \dot{f}, \ddot{f})$  from the signal as they are the key parameters for inferring neutron star properties. As an initial attempt to study the errors in these parameters from a CGW detection, we use a simple Fisher information matrix approach similar to [20, 21, 25]. This approach is strictly valid only in the case of high-signal-to-noise ratios. It has other issues like the possibility of a singular or ill-conditioned Fisher information matrix [30]. Nevertheless, due to its computational simplicity, we use this approach to get a quantitative picture. A comprehensive study using Bayesian inference is expected to give more robust results and is left to future work.

For long observation duration compared to a day, the parameter space metric over the phase parameters  $(f, \dot{f}, \ddot{f})$  is approximately given by the "phase metric" [31]:

$$g_{ij}(\lambda) = \left\langle \frac{\partial \phi}{\partial f^i} \frac{\partial \phi}{\partial f^j} \right\rangle - \left\langle \frac{\partial \phi}{\partial f^i} \right\rangle \left\langle \frac{\partial \phi}{\partial f^j} \right\rangle, \quad (6)$$

where  $(f, \dot{f}, \ddot{f}) \equiv (f^0, f^1, f^2)$  and the time average operator  $\langle \ \rangle$  is defined as:

$$\langle x(t) \rangle = \frac{1}{T} \int_{-T/2}^{T/2} x(t) dt, \quad (7)$$

where  $T$  is the total observation time (assuming 100% duty cycle). The metric quantifies the "distance" between two points in the parameter space. The inverse of the Fisher information matrix (which is also the covariance matrix), in terms of the metric, is:

$$\Gamma^{ij} = \frac{g^{ij}}{\rho^2}. \quad (8)$$

In Eq (8)  $\rho$  is the signal-to-noise ratio, which for a year or longer observation time, can be averaged over  $\iota$  and  $\psi$  and sky position [26]:

$$\rho^2 = \frac{4}{25} \frac{h_0^2 T}{S_h(f)}, \quad (9)$$

$$\rho^2 = \frac{4}{25} \frac{T}{\mathcal{D}^2}, \quad (10)$$

where  $S_h$  is the single-sided spectral density of the strain noise in the detector, and in Eq (10),  $\mathcal{D}$  is the "sensitivity depth" [32, 33]:

$$\mathcal{D} = \frac{\sqrt{S_h(f)}}{h_0}. \quad (11)$$

The covariance matrix is calculated from Eq (8), using Eq (6) and Eq (10):

$$\Sigma(f, \dot{f}, \ddot{f}) = \frac{\mathcal{D}^2}{\pi^2} \begin{pmatrix} \frac{1875}{16T^3} & 0 & -\frac{7875}{2T^5} \\ 0 & \frac{1125}{T^5} & 0 \\ -\frac{7875}{2T^5} & 0 & \frac{157500}{T^7} \end{pmatrix} \quad (12)$$

Now, the only relevant amplitude parameter is  $h_0$ . The error in  $h_0$  is calculated using the Fisher information matrix over the amplitude parameters  $\mathcal{A}_i$ 's and the coordinate transformation from  $\mathcal{A}_i$  to  $(h_0, \iota, \psi, \phi_0)$ [34]. For year-long observation, the error can be averaged over the sky position and  $\psi$  [21]:

$$\sigma(h_0) \approx \frac{4.08 \mathcal{D} h_0}{\sqrt{T}} \frac{\sqrt{2.59 + \cos(\iota)^2}}{1 - \cos(\iota)^2}. \quad (13)$$

Note that Eq (13) is singular at  $(\iota = 0 \text{ or } \pi)$  due to the coordinate transformation from  $\mathcal{A}_i$  to  $(h_0, \iota, \psi, \phi_0)$ . For this reason, we can't average over  $\iota$  with a prior range that includes 0 and  $\pi$ . Thus, In this work, we assume  $\cos(\iota)$  lies in the range of  $[-0.9, 0.9]$ , ignoring the small probability of cases where  $|\cos(\iota)| \approx 1$ .

### III. PARAMETER ESTIMATION FRAMEWORK

In this section we develop two different frameworks based on [21] and [25], to infer three neutron star properties: its principal moment of inertia ( $I$ ), the component of magnetic dipole moment perpendicular to the rotation axis ( $m_p$ ) and a parameter ( $\alpha$ ) which is related to the saturation amplitude ( $\alpha_s$ ) by  $\alpha = \alpha_s M R^3 \tilde{J}$ . In both cases, we assume that the

spin-down of the star is due to magnetic dipole radiation and gravitational wave emission (via r-mode current quadrupole). We ignore the minor effects of magnetic fields of the order  $10^{15}$  G or less, see section (VI) for more details. In the first scenario, we explore a framework similar to [21], where the distance is estimated from electromagnetic observations to 20% accuracy. The second scenario is relevant for targeted searches, where the rotational frequency of the star is known. As mentioned earlier the frequency of a r-mode signal varies slightly from  $f = \frac{4}{3}f_{rot}$ . This variation in frequency is quantified in terms of  $\kappa$  (see section III B), which satisfies universal relations with compactness [28] and the dimensionless tidal deformability [35]. We use the first universal relation to infer the distance of the star from CGW signals directly [25] along with the macroscopic properties mentioned above.

### A. Framework 1: Distance estimated from electromagnetic observations

Balancing the spin-down power with the luminosity of electromagnetic and gravitational radiation gives:

$$\left. \frac{dE}{dt} \right|_{EM} + \left. \frac{dE}{dt} \right|_{GW} = - \left. \frac{dE}{dt} \right|_{rot}. \quad (14)$$

The rotational kinetic energy is taken to be that of a rotating sphere:

$$\left. \frac{dE}{dt} \right|_{rot} = \frac{9}{4} \pi^2 I f \dot{f}. \quad (15)$$

The luminosity of an electromagnetic dipole is given by:

$$\left. \frac{dE}{dt} \right|_{EM} = \frac{27\pi^4}{8c^3\mu_0} \frac{m_p^2 f^4}{I}, \quad (16)$$

where  $\mu_0$  is vacuum permeability. The gravitational wave luminosity for r-mode is [15]:

$$\left. \frac{dE}{dt} \right|_{GW} = \frac{1024\pi^9 G}{25 c^7} \alpha^2 f^8. \quad (17)$$

To simplify the expressions we introduce the following constants,

$$K_d = \frac{3\pi^2}{2c^2\mu_0} \quad K_{gw} = \frac{4096\pi^7 G}{225c^7} \quad K_{h_0} = \sqrt{\frac{512\pi^7 G}{5 c^5}}. \quad (18)$$

The spin-down equations are then given by:

$$\dot{f} = - \frac{K_d m_p^2}{I} f^3 - \frac{K_{gw} \alpha^2}{I} f^7. \quad (19)$$

Differentiating (19) we get:

$$\ddot{f} = -3\frac{K_d m_p^2}{I} f^2 \dot{f} - 7\frac{K_{gw} \alpha^2}{I} f^6 \dot{f}. \quad (20)$$

As  $(h_0, f, \dot{f}, \ddot{f})$  are independently estimated from the CGW signal, we can solve Eq (2), Eq (19), and Eq (20) to get:

$$\alpha = \frac{r h_0}{K_{h_0} f^3}, \quad (21)$$

$$I = \frac{-4K_{gw} h_0^2 r^2 f}{K_{h_0} \dot{f} (n-3)}, \quad (22)$$

$$m_p = \sqrt{\frac{K_{gw} h_0^2 r^2 (7-n)}{K_d K_{h_0}^2 f^2 (n-3)}}. \quad (23)$$

Note that  $r$  is the distance to the star and the parameter  $\alpha$  is independent of  $n$  and is related to the saturation amplitude by:

$$\alpha = \alpha_s M R^3 \tilde{J}. \quad (24)$$

One requires mass and radius measurements from electromagnetic observations to estimate the saturation amplitude from observation. The negative sign in Eq (22) exists as  $\dot{f} < 0$ . Eqs (21) - (23) are valid only when  $3 < n < 7$ . This reflects the assumption that the spin-down of the star is due to magnetic dipole radiation and r-mode gravitational wave emission.

The differential error of any quantity is given by [21]:

$$\sigma(A)^2 = \Sigma_{x,y} \frac{\partial A}{\partial x} \frac{\partial A}{\partial y} cov(x, y), \quad (25)$$

where  $x, y \in (h_0, f, \dot{f}, \ddot{f})$  and "cov" represents the covariance of x and y. The errors of the neutron star properties can be calculated from Eq (25), (12), and (13) [21]:

$$\frac{\sigma(\alpha)^2}{\alpha^2} = \frac{\sigma(r)^2}{r^2} + \frac{\sigma(h_0)^2}{h_0^2} + \frac{16875\mathcal{D}^2}{16\pi^2 f^2 T^3}, \quad (26)$$

$$\frac{\sigma(I)^2}{I^2} = \frac{4\sigma(r)^2}{r^2} + \frac{4\sigma(h_0)^2}{h_0^2} + \frac{16875\mathcal{D}^2}{16\pi^2 f^2 (n-3)^2 T^3}, \quad (27)$$

$$\frac{\sigma(m_p)^2}{m_p^2} = \frac{\sigma(r)^2}{r^2} + \frac{\sigma(h_0)^2}{h_0^2} + \frac{1875\mathcal{D}^2 (n^2 - 9n + 15)^2}{16\pi^2 f^2 (n-5)^2 (n-3)^2 T^3}. \quad (28)$$

Note that the error in strain amplitude is inversely proportional to observation time ( $\sigma(h_0) \sim T^{-1/2}$ , see Eq (13)), therefore the errors asymptote to the error in distance as  $T \rightarrow \infty$ :

$$\lim_{T \rightarrow \infty} \frac{\sigma(\alpha)}{\alpha} = \frac{\sigma(r)}{r}, \quad (29)$$



$$\lim_{T \rightarrow \infty} \frac{\sigma(I)}{I} = \frac{2\sigma(r)}{r}, \quad (30)$$

$$\lim_{T \rightarrow \infty} \frac{\sigma(m_p)}{m_p} = \frac{\sigma(r)}{r}. \quad (31)$$

The factor of 2 in Eq (30) exists as  $I$  is proportional to  $r^2$ , whereas  $\alpha$  and  $m_p$  are proportional to  $r$ .

## B. Framework 2: Using universal relation to estimate distance

The frequency of the relevant ( $l = m = 2$ ) r-mode oscillation, under the slow-rotation approximation, is given by:

$$f = |2 - \kappa|f_{rot}, \quad (32)$$

where  $f_{rot}$  is the rotational frequency of the neutron star. For a slow-rotating Newtonian star:  $\kappa = \frac{2}{3}$ . Various factors like relativistic effects, rapid rotation and magnetic field affect the value of  $\kappa$ . It has been shown that the relativistic effect is the strongest factor [28] and that  $\kappa$  satisfies a universal relation with the compactness ( $C = \frac{M}{R}$ ) of the star, given by ([28, 35]):

$$\kappa = 0.667 - 0.478C - 1.11C^2. \quad (33)$$

The compactness of the star also satisfies a universal relation with the normalised moment of inertia ( $\bar{I} = \frac{I}{M^3}$ ) for slowly rotating stars ([36]):

$$\begin{aligned} \ln(\bar{I}) = & 0.8314C^{-1} + 0.2101C^{-2} + 3.175 \times 10^{-3}C^{-3} \\ & - 2.717 \times 10^{-4}C^{-4}, \end{aligned} \quad (34)$$

where Eq (34) is in geometric units ( $G = c = 1$ ).

For the case of targeted searches, we can use Eq (32) to calculate  $\kappa$  from a CGW detection. The universal relations can then be used to calculate the compactness and normalised moment of inertia. At this point assuming an equation of state of the neutron star lets us calculate its moment of inertia by varying the central density to match the compactness and the normalised moment of inertia. Note that the  $\bar{I} - C$  relation (34) is not actually required to determine the moment of inertia as there exists a one-to-one relation between the moment of inertia and compactness for a given equation of state. We still use Eq (34) in this framework as in the case where mass measurements are available for the star, Eq (34)

allows us to measure the moment of inertia independent of the EOS. Check section VIC for a more detailed discussion. We can then get the distance to the star by rearranging Eq (22), using which the remaining parameters are calculated. This is similar to [25], where they use universal relations with normalised tidal deformability instead of the compactness of the star.

The error in  $\kappa$  is given by ([25]):

$$\sigma(\kappa)^2 = \frac{f^2}{f_{rot}^2} \left[ \frac{\sigma(f)^2}{f^2} + \frac{\sigma(f_{rot})^2}{f_{rot}^2} \right]. \quad (35)$$

Then using the universal relations the error in the normalised moment of inertia is:

$$\begin{aligned} \frac{\sigma(\bar{I})^2}{\bar{I}^2} &= \frac{1}{C^2} (0.831C^{-1} + 0.420C^{-2} + 9.525 \times 10^{-3}C^{-3} \\ &\quad - 1.087 \times 10^{-3}C^{-4})^2 \times \frac{\sigma(\kappa)^2}{(0.478 + 2.22C)^2}, \end{aligned} \quad (36)$$

which is equal to the error in  $\sigma(I)/I$  given an equation of state. The error in the distance of the star, calculated from Eq (27) is then:

$$\frac{\sigma(r)^2}{r^2} = \frac{\sigma(I)^2}{4I^2} - \frac{\sigma(h_0)^2}{h_0^2} - \frac{16875\mathcal{D}^2}{64\pi^2 f^2 (n-3)^2 T^3}. \quad (37)$$

We can also estimate the error in  $\alpha$  and  $m_p$  via Eq's (26) - (28):

$$\frac{\sigma(\alpha)^2}{\alpha^2} = \frac{\sigma(I)^2}{4I^2} + \frac{(4n^2 - 24n + 35)}{4(n-3)^2} \frac{16875\mathcal{D}^2}{16\pi^2 f^2 T^3}, \quad (38)$$

$$\frac{\sigma(m_p)^2}{m_p^2} = \frac{\sigma(I)^2}{4I^2} + \frac{1875\mathcal{D}^2 (n^2 - 9n + 15)^2}{16\pi^2 f^2 (n-5)^2 (n-3)^2 T^3} - \frac{16875\mathcal{D}^2}{64\pi^2 f^2 (n-3)^2 T^3}. \quad (39)$$

Note that all the neutron star properties except the distance are independent of the signal strain amplitude ( $h_0$ ).

#### IV. MONTE CARLO SIMULATION

In this section we explain how we use Monte Carlo simulations to study the errors in the three inferred parameters. In Section IV A, we talk about Monte Carlo simulations for the first framework (Section III A). Then, in Section IV B, we discuss the procedure of Monte Carlo simulations for the second framework (Section III A).

### A. Framework 1

Here the parameters  $h_0, f, \dot{f}, n$ , and  $r$  are required for inference and their errors depend on  $\mathcal{D}, T, \iota, h_0$ , and  $\Delta r$ . We assume a distance of 1 Kpc is estimated via electromagnetic observations with a 20% observational error, which is consistent with the previous study [21].

We also choose to input values of  $I$ , instead of  $h_0$  through rearrangement of Eq (22), similar to [21]. This is because the results that directly depend on  $h_0$  can be viewed as a stronger or weaker signal. On the other hand, choices of  $I$  relate to the internal physics of the star. Even though a larger  $I$  means a stronger signal (as  $I \sim MR^2$ ), the strength also depends on other factors like  $\alpha_s$  and  $r$ . A signal from a neutron star is simulated by 9 parameters  $f_{\text{in}}, \dot{f}_{\text{in}}, \ddot{f}_{\text{in}}, I_{\text{in}}, r_{\text{in}}, T_{\text{in}}, \mathcal{D}_{\text{in}}, \cos(\iota)_{\text{in}}$ , and  $\Delta r$ . Using these we calculate the input properties  $I_{\text{in}}, \alpha_{\text{in}}$ , and  $m_{p_{\text{in}}}$  using Eqs (21) - (23). Then the errors  $(\delta f, \delta \dot{f}, \delta \ddot{f})$  are drawn from a multivariate normal distribution whose covariance matrix is given by Eq (12). Similarly, the error  $(\delta h_0)$  is drawn from a normal distribution with the standard deviation given by Eq (13). All other covariances are assumed to be zero. Then the output parameters are given by:

$$\begin{aligned} f^{\text{out}} &= f^{\text{in}} + \delta f, & \dot{f}^{\text{out}} &= \dot{f}^{\text{in}} + \delta \dot{f}, \\ \ddot{f}^{\text{out}} &= \ddot{f}^{\text{in}} + \delta \ddot{f}, & h_0^{\text{out}} &= h_0^{\text{in}} + \delta h_0. \end{aligned} \tag{40}$$

Using these output parameters we calculate  $I_{\text{out}}, \alpha_{\text{out}}$ , and  $m_{p_{\text{out}}}$ , which is then compared with  $I_{\text{in}}, \alpha_{\text{in}}$ , and  $m_{p_{\text{in}}}$ . This process is iterated  $10^6$  times.

#### 1. Choice of input parameters

Here we discuss the choice of the ranges/values of the 9 input parameters mentioned above. We consider an observation time of 0.5 – 4 years, as gravitational wave detectors observing runs last at least a year. A fixed  $r_{\text{in}}$  of 1 Kpc is assumed. This is expected to be within the range where all-sky searches are sensitive to neutron stars with  $\alpha_s > 10^{-4}$  and  $f > 100$  Hz. An error of 20% is assumed in the distance measurement, which is not unreasonable for current and next-generation radio telescopes [37, 38].

Unlike [21], we only explore a sensitivity depth of  $\mathcal{D}_{\text{in}} = 30 \text{ Hz}^{-1/2}$ , which is typical for all-sky searches [32]. This must be interpreted as a signal being detected with a relatively low computational cost. A more sensitive follow-up analysis would significantly increase the

signal-to-noise ratio. Check [21] for details on how stability time, the time taken for the parameter errors to reach within 10% of the distance error, varies as a function of sensitivity depth. One could also use  $S_h(f)$  of current and future gravitational wave detectors [25], but we don't take this approach.

We draw the moment of inertia from the widely accepted range for neutron stars of  $I_{\text{in}} = [1, 3] \times 10^{38}$  Kg-m<sup>2</sup> [39–41],  $\cos(\iota)_{\text{in}}$  is drawn from  $[-0.9, 0.9]$  and  $n_{\text{in}}$  is drawn from  $[3, 7]$ , based on our assumption of the spin-down mechanism. The range of values assumed for  $f_{\text{in}}$  and  $\dot{f}_{\text{in}}$  is given by:

$$f_{\text{in}} = [30, 700] \text{ Hz}, \quad \dot{f}_{\text{in}} = [-10^{-8}, -10^{-12}] \text{ Hz s}^{-1}, \quad (41)$$

where the range of  $f$  is slightly smaller than current all-sky surveys [42], as for higher frequencies we would have to include the corrections to r-mode frequency due to rapid rotation [28]. These ranges almost translate to surface magnetic fields of the order  $10^{11} - 10^{15}$  G. We also restrict saturation amplitude to values between  $[10^{-7}, 10^{-1}]$ , which is consistent with current numerical simulations [13, 43]. For each iteration we draw  $I_{\text{in}}, f_{\text{in}}, \dot{f}_{\text{in}}, n_{\text{in}}$ , and  $\cos(\iota)_{\text{in}}$  from a uniform distribution, calculate  $h_{\text{in}}$  via Eq (22) and then use it to calculate  $\alpha_{\text{in}}$ , and  $m_{p_{\text{in}}}$  via Eq (21) and Eq (23).

## 2. Output Parameters

Post choosing values for the input parameters, we convert  $\alpha$  into estimates of  $\alpha_s$  by using Eq (24) and fiducial values for  $M = 1.4M_{\odot}$ ,  $R = (5I_{\text{in}}/2M)^{1/2}$  and  $\tilde{J} = 0.01635$  [11]. The output parameters  $h_{\text{out}}, f_{\text{out}}, \dot{f}_{\text{out}}$ , and  $\ddot{f}_{\text{out}}$  are then calculated via Eq (40). The output braking index  $n_{\text{out}}$  is then calculated using Eq (5). We ignore cases where  $\alpha_s \notin [10^{-8}, 10^{-1}]$  and  $n_{\text{out}} \notin [3, 7]$ . The condition on  $n_{\text{out}}$  is required for the calculation of  $(I_{\text{out}}, \alpha_{\text{out}}, m_{p_{\text{out}}})$  and only a small fraction of the data is lost ( $\sim 1\%$ ), for observation time greater than a year. Due to the restriction on  $\alpha_s$ , we lose around 8% to 16% of data as  $n_{\text{in}}$  increases from 3 to 7. This is due to an increase in the number of cases where  $\alpha_s > 10^{-1}$  as  $n_{\text{in}}$  is close to 7. Although a significant chunk of data is lost, we still obtain key quantitative trends (section [V]).

To compare the output and input parameters we use the median relative error:

$$\epsilon(P) \equiv \text{median} \left\{ \left| \frac{P_{\text{out}} - P_{\text{in}}}{P_{\text{in}}} \right| \text{ with } P \in \{I, m_p, \alpha, r\} \right\}, \quad (42)$$

following [21]. For framework 1, we also normalise the error of  $(I, m_p, \alpha)$  by the median error in the distance ( $\epsilon(r) \approx 0.135$ ) [21]:

$$\tilde{\epsilon}(I) = \frac{\epsilon(I)}{2\epsilon(r)}, \quad \tilde{\epsilon}(\alpha) = \frac{\epsilon(\alpha)}{\epsilon(r)}, \quad \tilde{\epsilon}(m_p) = \frac{\epsilon(m_p)}{\epsilon(r)}. \quad (43)$$

## B. Framework 2

In this section, we discuss how we modify the Monte Carlo simulation for the second framework. Unlike the previous section, this framework depends on the choice of an equation of state of the star and is only relevant for targeted narrow-band searches.

The key parameters required for inference in this case are  $h_0, f, \dot{f}, n$ , and  $\kappa$  and their errors depend on  $\mathcal{D}, T, \iota, h_0$ , and  $\Delta f_{rot}$ . Here  $\Delta f_{rot}$  refers to the measurement error in the neutron star's rotation frequency from electromagnetic measurements. In this case, we directly input values of  $h_0$ , as we can't directly input values of any inherent neutron star properties. The 9 input parameters are then  $f_{in}, \dot{f}_{in}, \ddot{f}_{in}, h_{0in}, \kappa_{in}, T_{in}, \mathcal{D}_{in}, \cos(\iota)_{in}$ , and  $\Delta f_{rot}$ , using which we calculate the normalised moment of inertia  $\bar{I}$  via Eq (34). An equation of state is then assumed to calculate the input properties  $I_{in}, r_{in}, \alpha_{in}$ , and  $m_{pin}$  via Eq's (21) - (23). We then calculate the output parameters similar to section IV A and this is iterated  $10^5$  times (An order less than the previous case due to computational cost).

### 1. Choice of input parameters

Now we discuss the choice of the ranges/values of the input parameters mentioned above. We consider a similar observation time to the previous case. A range of  $[10^{-25} - 10^{-27}]$  is explored for  $h_{0in}$ , as this range includes signals that current and future detectors can potentially detect on narrow band searches [15, 44]. The range of  $h_{0in}$  can be interpreted as a range in the input distance ( $r_{in}$ ) of the star since it is the sole parameter that depends on the strain amplitude ( $h_0$ ). The value of  $\kappa$  is drawn from  $[0.45, 0.60]$ , based on theoretical considerations [28]. We explore a sensitivity depth of  $\mathcal{D}_{in} = 100 \text{ Hz}^{-1/2}$ , which is reasonable for narrow-band searches [32, 45]. Similar to the previous case,  $\cos(\iota)$  is drawn from  $[-0.9, 0.9]$  and  $n_{in}$  is drawn from [3, 7]. The range of values assumed for  $f_{in}$  and  $\dot{f}_{in}$  is given by:

$$f_{in} = [30, 500] \text{ Hz}, \quad \dot{f}_{in} = [-10^{-8}, -10^{-12}] \text{ Hz s}^{-1}, \quad (44)$$

which is a smaller parameter space in  $f$  in comparison to the previous case, as the universal relation (Eq (34)) is only valid for slow rotations. We estimate the rotation frequency of the star from Eq (32) and assume a measurement error ( $\Delta f_{rot}$ ) of 0.1%, although pulsar frequencies are measured with much higher accuracy [46]. These ranges almost translate to similar values of magnetic field and saturation amplitude as found in section IV A. For each iteration we draw  $(\kappa_{in}, h_{0in}, f_{in}, \dot{f}_{in}, n_{in}, \cos(\iota)_{in})$  from a uniform distribution, calculate  $\bar{I}_{in}$  via Eq (34) and then use it to calculate  $(r_{in}, I_{in}, \alpha_{in}, m_{p_{in}})$ . Note that one can estimate  $M$  and  $R$  from  $\bar{I}$  and thus calculate the saturation amplitude  $\alpha_s$  directly. This is used to ignore the cases where the saturation amplitude is not within  $[10^{-7}, 10^{-1}]$ .

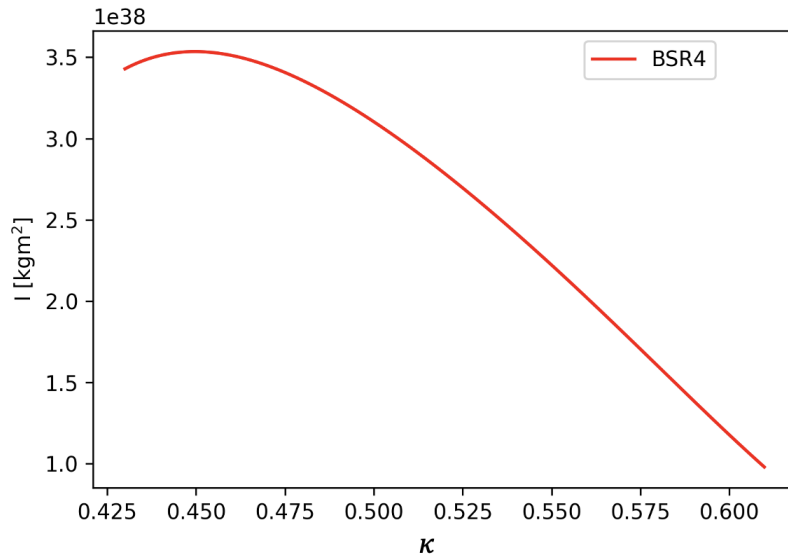


FIG. 1. Moment of inertia ( $I$ ) as a function of  $\kappa$  for the BSR4 equation of state.

In this work, we use the BSR4 ([47, 48]) equation of state to calculate the moment of inertia via the RNS code [49]. Figure 1 shows the dependence of moment of inertia as a function of  $\kappa$  for the BSR4 equation of state. This dependency is calculated by varying the central density to match the normalised moment of inertia for each  $\kappa$  value. Check [25] to see how this dependence varies for other realistic equations of state.

## 2. Output parameters

Similar to section IV A, we ignore cases where  $\alpha_s \notin [10^{-8}, 10^{-1}]$  and  $n_{out} \notin [3, 7]$ . Due to this, we again lose around 8% to 16% of data as  $n_{in}$  increases from 3 to 7. We again use

the median relative error (Eq (42)) to compare the input and output parameters, but we don't normalise the error with the 0.1% error assumed for the rotational frequency. This is because the error depends on other input parameters, as  $T \rightarrow \infty$ :

$$\lim_{T \rightarrow \infty} \frac{\sigma(\bar{I})}{\bar{I}} = \frac{1}{C} \left( 0.831C^{-1} + 0.420C^{-2} + 9.525 \times 10^{-3}C^{-3} - 1.087 \times 10^{-3}C^{-4} \right) \frac{f}{f_{\text{rot}}} \frac{\sigma(f_{\text{rot}})}{(0.478 + 2.22C)}.$$

## V. RESULTS

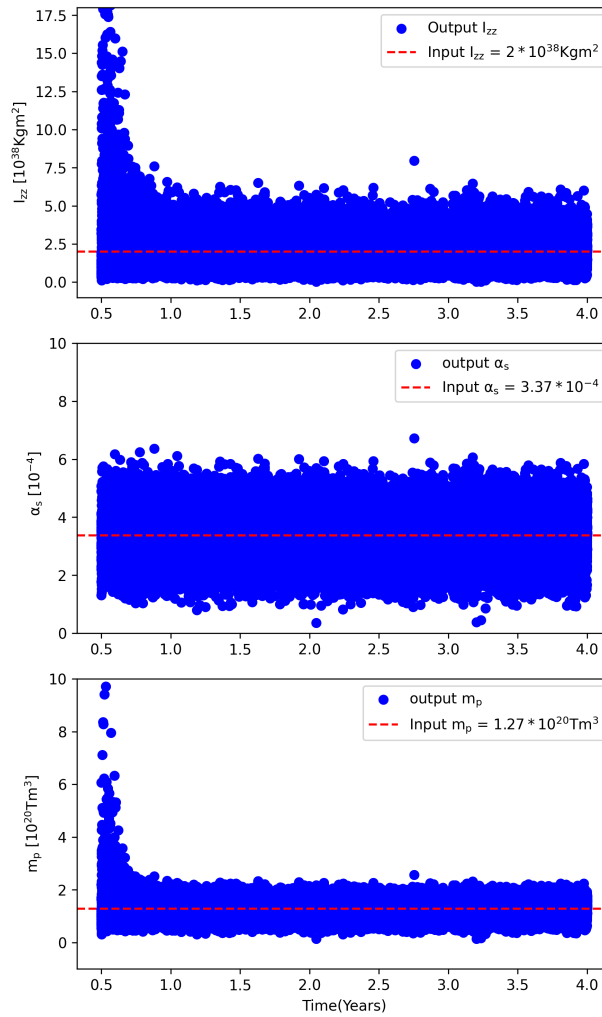


FIG. 2. Inference via framework 1:  $(I_{\text{out}}, \alpha_{s\text{out}}, m_{p\text{out}})$  converges to  $(I_{\text{in}}, \alpha_{s\text{in}}, m_{p\text{in}})$  with increase in observation time. Here the input parameters are  $f = 300 \text{ Hz}$ ,  $\dot{f} = -10^{-9} \text{ Hz s}^{-1}$ ,  $n = 3.1$ ,  $\mathcal{D} = 30 \text{ Hz}^{-1/2}$ ,  $\cos(\iota) = 0$  and  $I = 2 \times 10^{38} \text{ kg-m}^2$ . We convert the value of  $\alpha$  into fiducial estimates of  $\alpha_s$  by setting  $M = 1.4M_{\odot}$ ,  $\tilde{J} = 0.01635$  and  $R = \sqrt{5I/2M}$ .

In this section, we present the results of the Monte Carlo error estimation study mentioned in section IV. We analyse the dependence of errors on various factors like observation time and braking index and, also present a comparative analysis between both frameworks.

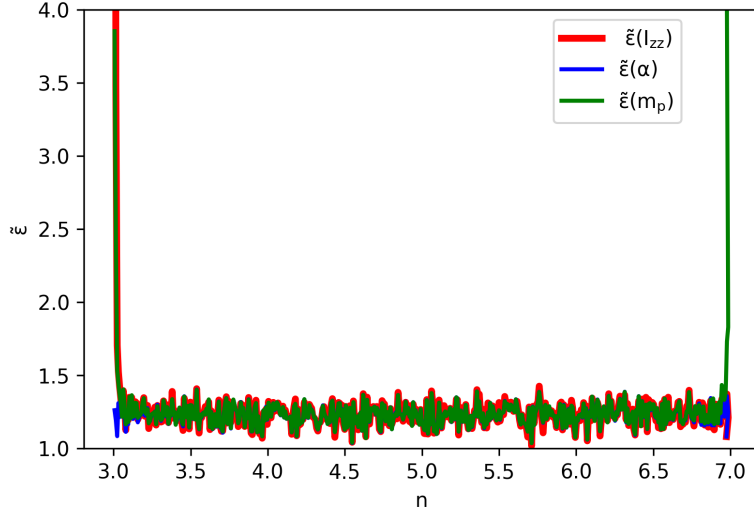


FIG. 3. Inference via framework 1: Normalised relative errors ( $\tilde{\epsilon}$ ) as a function of the braking index  $n$  post-down-sampling. Here the input parameters are  $f = 300$  Hz ,  $\dot{f} = -10^{-9}$  Hz s $^{-1}$ ,  $T = 1$  year,  $\mathcal{D} = 30$  Hz $^{-1/2}$ ,  $\cos(\iota) = 0$  and  $I = 2 \times 10^{38}$  Kg-m $^2$ .

Unlike [21], the errors inferred via the first framework are dominated by the error in distance for even an observation time of  $T = 0.5$  years. This feature is seen for all values of the braking index except close to the extremes (3 or 7). Figure 2 shows how the neutron star properties inferred via the first framework, converge to their actual values as observation time increases for  $n = 3.1$ . The input values for the parameters are  $I = 2 \times 10^{38}$  Kg-m $^2$  ,  $\alpha = 3.69 \times 10^{37}$  ( converted into fiducial estimates:  $\alpha_s = 3.37 \times 10^{-4}$ ) and  $m_p = 1.27 \times 10^{20}$  Tesla-m $^2$ . As expected from theoretical considerations (Eqs (26) - (31)), the errors in the parameters ( $I, m_p$ ) decrease with observation time and for  $T > 1$  years we see the error saturates to the error in the distance measurement. We do not observe this pattern for alpha ( $\alpha$ ) as it is independent of the braking index and the error in the distance measurement dominates the error in alpha even for an observation time of  $T = 0.5$  years. We can check



this by substituting all the assumed input parameters in Eq (26):

$$\begin{aligned} \frac{\sigma(\alpha)^2}{\alpha^2} &= \frac{\sigma(r)^2}{r^2} + \frac{\sigma(h_0)^2}{h_0^2} + \frac{16875\mathcal{D}^2}{16\pi^2 f^2 T^3} \\ &= 0.04 + 0.0025 + 2.75 \times 10^{-22}, \end{aligned} \quad (45)$$

where the observation time is  $T = 0.5$  years.

Figure 3 shows the dependence of normalised relative errors ( $\tilde{\epsilon}$ ) on the neutron star's braking index ( $n$ ), where signals are inferred via the first framework. It is for signals with  $f_{\text{in}} = 300$  Hz,  $\dot{f}_{\text{in}} = -10^{-9}$  Hz s $^{-1}$ ,  $T_{\text{in}} = 1$  year,  $\mathcal{D}_{\text{in}} = 30$  Hz $^{-1/2}$ , and  $I_{\text{in}} = 2 \times 10^{38}$  Kg-m $^2$ . The moment of inertia ( $I$ ) is best estimated at ( $n \approx 7$ ), where the spin-down is caused mostly due to gravitational waves. The perpendicular component of the dipole moment is estimated with the best accuracy when the spin-down is caused by both electromagnetic radiation and gravitational waves. As expected, the median error in the parameter alpha ( $\alpha$ ) does not depend on the braking index.

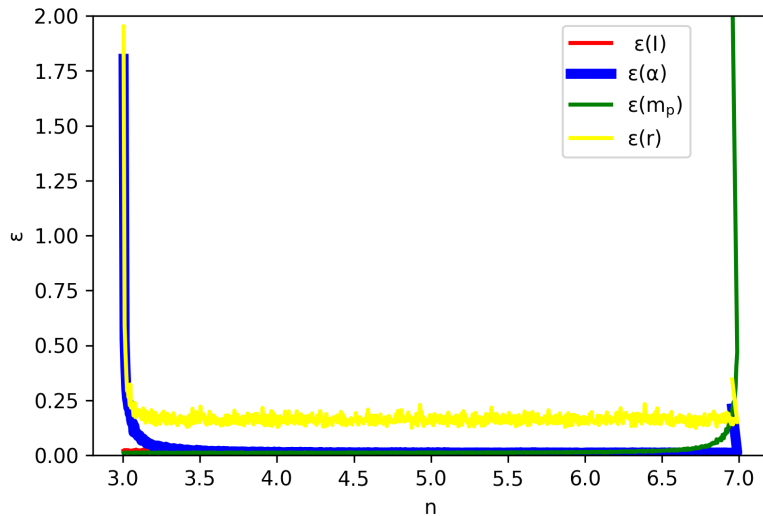


FIG. 4. Inference via framework 2 : Relative errors ( $\epsilon$ ) as a function of braking index  $n$  post-down-sampling. Here the input parameters are  $h_0 = 1 \times 10^{-26}$ ,  $f = 300$  Hz,  $\dot{f} = -10^{-9}$  Hz s $^{-1}$ ,  $T = 1$  year,  $\mathcal{D} = 100$  Hz $^{-1/2}$ ,  $\cos(\iota) = 0$  and  $\kappa = 0.56$ .

Figure 4 shows the sharp contrast in the dependence of median errors ( $\epsilon$ ) on the braking index ( $n$ ) when we infer parameters via the second framework. This is shown for signals with  $h_{0\text{in}} = 1 \times 10^{-26}$ ,  $f_{\text{in}} = 300$  Hz,  $\dot{f}_{\text{in}} = -10^{-9}$  Hz s $^{-1}$ ,  $T_{\text{in}} = 1$  year,  $\mathcal{D}_{\text{in}} = 100$  Hz $^{-1/2}$ ,

and  $\kappa_{\text{in}} = 0.56$  (which implies  $I_{\text{in}} \approx 2 \times 10^{38} \text{ Kg-m}^2$ ). In this framework, the moment of inertia is independent of the breaking index as it is directly inferred from the frequency of the signal. The distance of the star ( $r$ ) and the parameter  $\alpha$  are best estimated at  $n \approx 7$ , and the perpendicular component of the dipole moment can be best estimated at around  $n \approx 3$ . We also observe the median error in distance saturates at a greater value than other parameters as it is the only parameter that directly depends on the strain amplitude ( $h_0$ ). For inference via the second framework, the median errors in  $\alpha$  can be interpreted as median errors in  $\alpha_s$ , as one can directly estimate ( $\alpha_s$ ) in this framework (Section IV B 2).

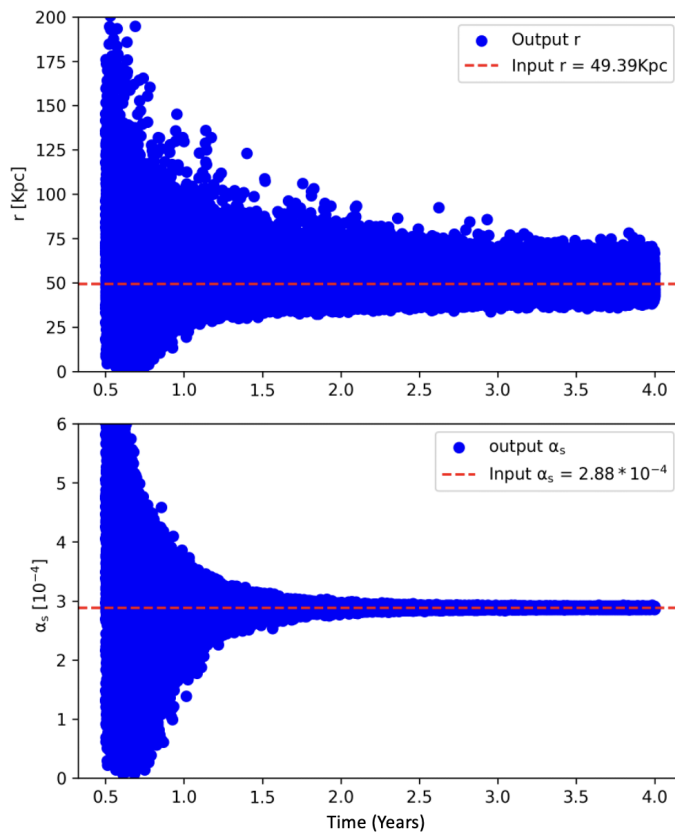


FIG. 5. Inference via framework 2:  $(r_{\text{out}}, \alpha_{\text{out}})$  converges to  $(r_{\text{in}}, \alpha_{\text{in}})$ . Here the inputs are  $h_{0\text{in}} = 1 \times 10^{-26}$ ,  $f = 300 \text{ Hz}$ ,  $\dot{f} = -10^{-9} \text{ Hz s}^{-1}$ ,  $n = 3.1$ ,  $\mathcal{D} = 100 \text{ Hz}^{-1/2}$ ,  $\cos(\iota) = 0$  and  $\kappa = 0.56$ .

In figure 5, we show the convergence of  $(r_{\text{out}}, \alpha_{s\text{out}})$  to  $(r_{\text{in}}, \alpha_{s\text{in}})$  for signals with  $h_0 = 1 \times 10^{-26}$ ,  $f_{\text{in}} = 300 \text{ Hz}$ ,  $\dot{f}_{\text{in}} = -10^{-9} \text{ Hz s}^{-1}$ ,  $n_{\text{in}} = 3.1$ ,  $\mathcal{D}_{\text{in}} = 100 \text{ Hz}^{-1/2}$ ,  $\cos(\iota)_{\text{in}} = 0$  and  $\kappa_{\text{in}} = 0.56$ . We observe the expected convergence of the parameters with the increase in observation time. The parameter  $\alpha_s$  saturates at an observation time of  $T > 2$  years due

to the 0.1% error in the rotation frequency. In comparison, the distance measurement is dominated by the error in  $h_0$  even for  $T > 4$  years.

Figure 6 shows the normalised relative errors  $\tilde{\epsilon}(I)$ ,  $\tilde{\epsilon}(\alpha)$ ,  $\tilde{\epsilon}(m_p)$  as function of frequency ( $f$ ) and it's derivative ( $\dot{f}$ ), for three values of braking index. The median errors are for parameters inferred via the first framework and have been taken over the sampled region of  $I$  and  $\cos(\iota)$  mentioned in section IV A 1. These errors are for signals with an observation time of  $T = 1$  year and detected with  $\mathcal{D} = 30Hz^{-1/2}$ , which is relevant for a signal detected in an all-sky search.

In figure 7 we plot the relative errors  $\epsilon(r)$ ,  $\epsilon(\alpha)$ ,  $\epsilon(m_p)$  ( $\epsilon(I)$  is not shown) as function of braking index ( $n$ ), frequency ( $f$ ) and it's derivative ( $\dot{f}$ ), for parameters inferred via the second framework. As mentioned earlier  $\epsilon(\alpha) \equiv \epsilon(\alpha_s)$ . These median errors are also taken over the sampled region of  $h_0$  and  $\cos(\iota)$  mentioned in section IV B 1. These errors are for signals with an observation time of  $T = 1$  year and detected with  $\mathcal{D} = 100 Hz^{-1/2}$ , which is relevant for a signal detected in a narrow band search.

Both fig 6 and fig 7 show that the errors in all inferred properties are minimum for high spin-down rates ( $\dot{f} \approx -10^{-8} Hz s^{-1}$  and low frequency ( $f \approx 100 Hz$ )). For stars which are spinning down slowly ( $\dot{f} < -10^{-11}$ ), the errors are so high that the condition  $3 < n_{out} < 7$  cannot be satisfied. These features that are common among both frameworks are also the case for signals produced due to mountains on a neutron star and when an inference strategy similar to the first framework is used [21]. In addition, we identify a white region characterized by low frequencies ( $f < 100Hz$ ) and high spin-down rates ( $\dot{f} > -10^{-9} Hz s^{-1}$ ), whose size is minimal for  $n \approx 3$  but gets larger as  $n \approx 7$ . This region corresponds to instances where the condition  $[\alpha_{sin} < 10^{-1}]$  is not met.

Fig 6 also suggests that a normalised relative error  $\tilde{\epsilon} \leq 1.2$  can be achieved for most of the parameter space ( $f, \dot{f}$ ) for all sky searches. This implies (via Eqn (43)) an error of 32% in  $I$  and a 16% error in  $\alpha$  and  $m_p$ . The errors in  $\alpha$  are sufficiently small that converting the measured  $\alpha$  into fiducial estimates of  $\alpha_s$  (as mentioned in section IV A 2) would provide valuable insights into the damping mechanisms that limit the growth of the r-modes ([12–14, 43]). On the other hand, Fig 7 shows that framework 2 leads to much lower errors due to the high accuracy in pulsar frequency measurements. An error of 16% can be achieved in distance measurements which is comparable to electromagnetic observations [37]. We also note a sufficiently low error of at least 2% for  $I$  and at least 1% for both  $\alpha$  and  $m_p$  (refer

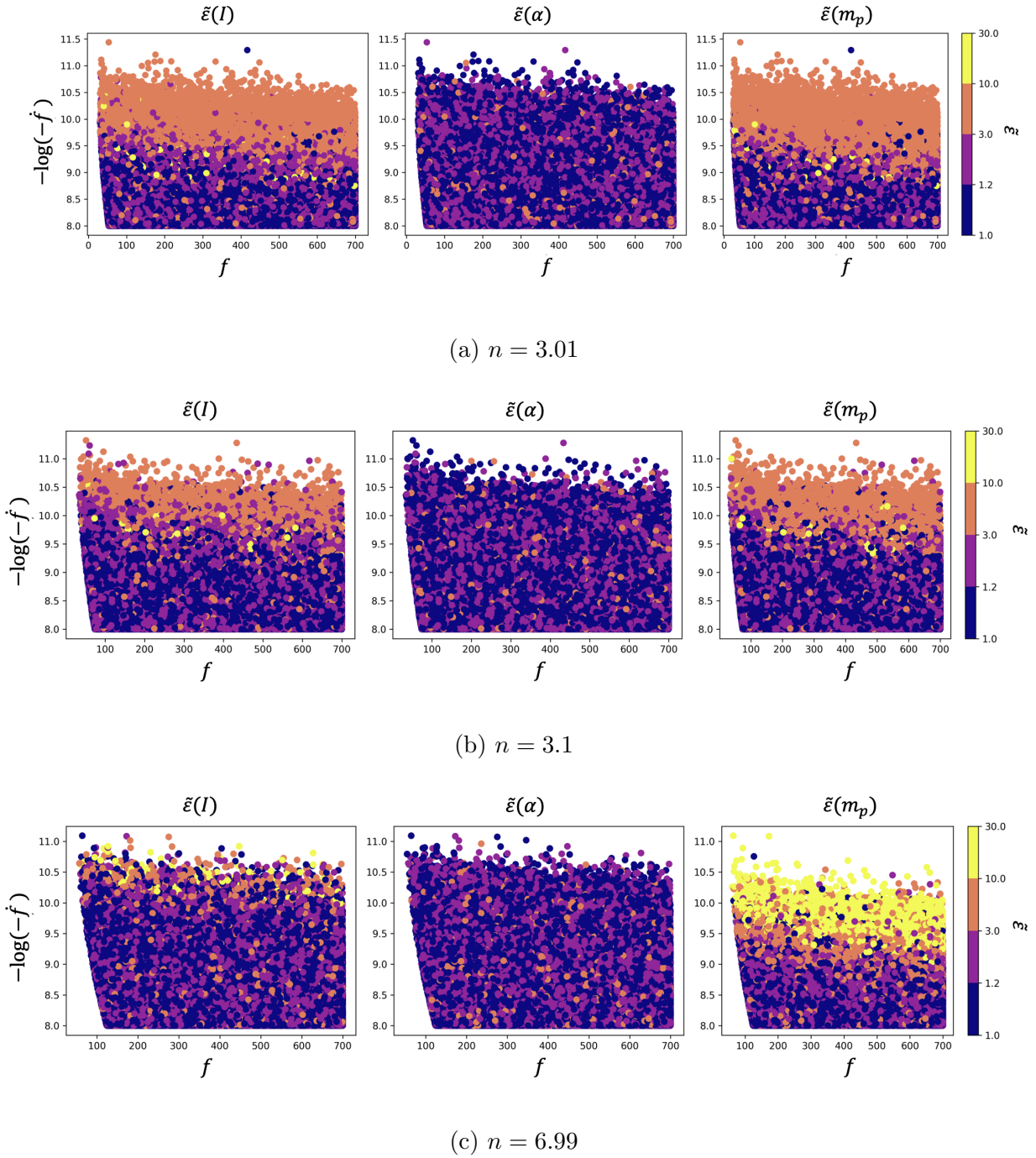


FIG. 6. Inference via framework 1: normalised relative errors  $\tilde{\epsilon}(I)$ ,  $\tilde{\epsilon}(\alpha)$ ,  $\tilde{\epsilon}(m_p)$ , for braking index  $n = 3.01, 3.1, 6.99$ , as function of frequency ( $f$ ) and it's derivative ( $\dot{f}$ ). Plotted are median errors for  $T = 1$  year and  $\mathcal{D} = 30 \text{ Hz}^{-1/2}$ . The white areas indicate regions where  $\tilde{\epsilon} > 30$  or  $n_{\text{out}} \notin [3, 7]$  or  $\alpha_s \notin [10^{-6}, 10^{-1}]$ . We used a total of  $10^6$  points.

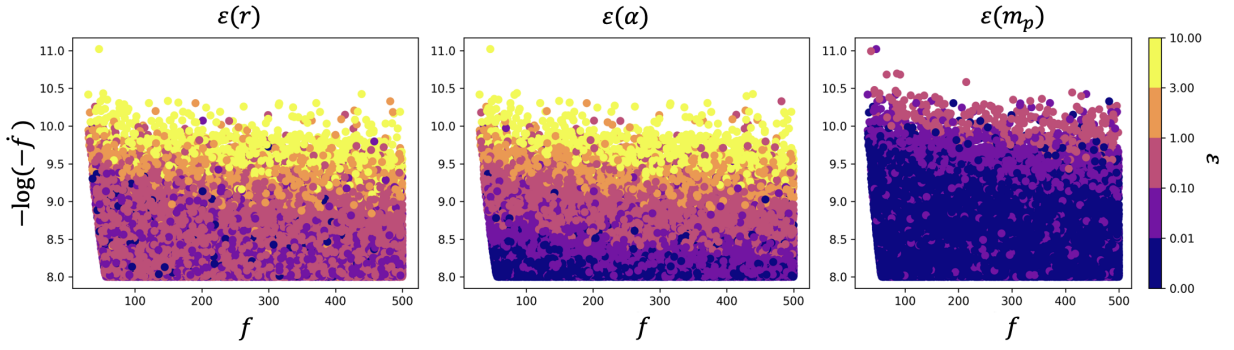
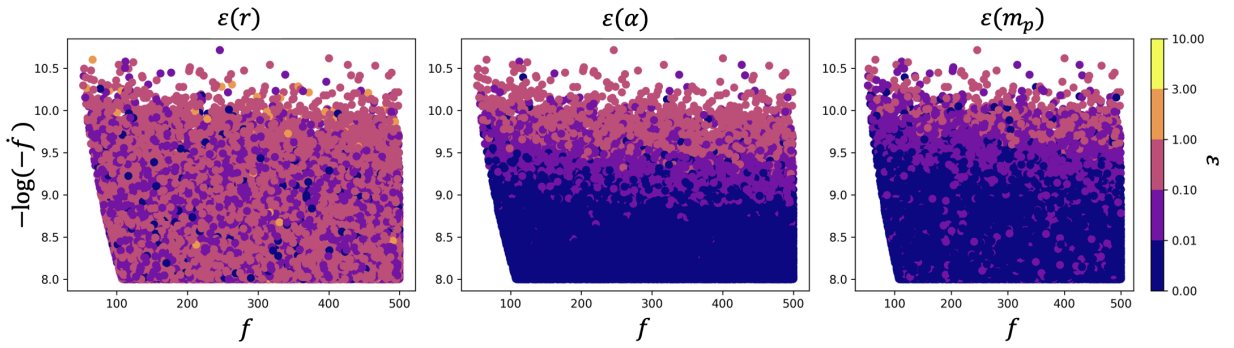
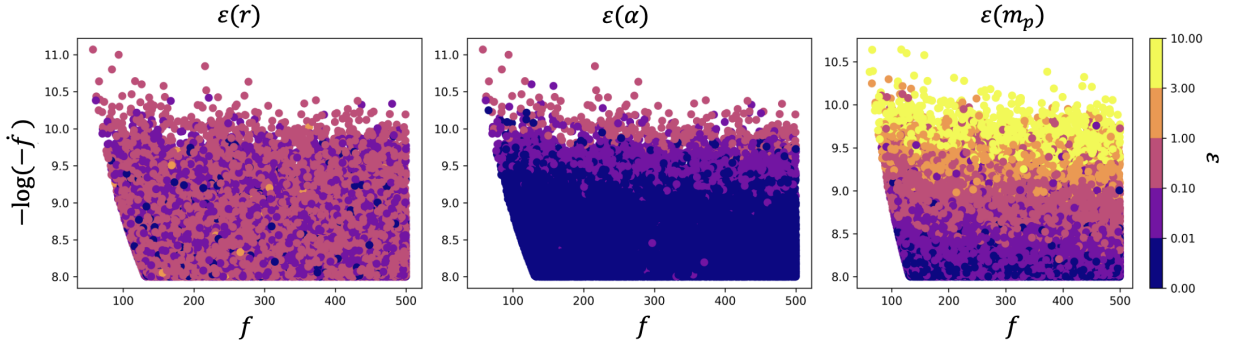
(a)  $n = 3.01$ (b)  $n = 4.0$ (c)  $n = 6.99$ 

FIG. 7. Inference via framework 2: Relative errors  $\tilde{\epsilon}(I)$ ,  $\tilde{\epsilon}(\alpha)$ ,  $\tilde{\epsilon}(m_p)$ , for braking index  $n = 3.01, 4, 6.99$ , as function of frequency ( $f$ ) and it's derivative ( $\dot{f}$ ). Plotted are median errors for  $T = 1$  year and  $\mathcal{D} = 100 \text{ Hz}^{-1/2}$ . The white areas indicate regions where  $\epsilon > 10$  or  $n_{out} \notin [3, 7]$  or  $\alpha_s \notin [10^{-6}, 10^{-1}]$ . Here we have used  $10^5$  points.

to Fig. 7), achievable with a sufficiently high spin-down rate. This is because the errors displayed in all properties, except the distance, do not directly depend on the strength  $h_0$  of the detected signal (as we have assumed  $\mathcal{D} = 100 \text{ Hz}^{\frac{1}{2}}$ ). However, this approach comes with the drawback of assuming a specific equation of state and works only for slowly rotating neutron stars. check VIB for the potential effects of magnetic field on this analysis.

## VI. DISCUSSION AND CONCLUSION

### A. Summary

In this article, we present an analysis similar to [21] of what properties can be inferred from neutron stars that radiate electromagnetic waves and detectable continuous gravitational waves produced by r-mode oscillations. We investigate two different frameworks. In the first framework, we assume the distance of the star is measured via electromagnetic observations with 20% accuracy. We then infer three neutron star properties: its principal moment of inertia ( $I$ ), the component of magnetic dipole moment perpendicular to the rotation axis ( $m_p$ ), and a parameter ( $\alpha$ ) which is related to the saturation amplitude by  $\alpha = \alpha_s MR^3 \tilde{J}$ . Unlike the signals produced due to mountains, for narrow-band searches, the signals due to r-mode oscillations give us information on an additional parameter ( $\kappa$ ) which satisfies universal relations with the compactness of the star [28, 35]. In the second framework, we use this and the  $I - C$  universal relations to directly measure the distance ( $r$ ) of the neutron star, along with the three parameters mentioned above. We then use a simple Fisher information matrix-based approach to present a quantitative error estimation study for parameters inferred via both frameworks.

Monte Carlo simulations typical for all-sky searches are done for the first framework, whereas simulations typical for narrow-band searches are done for the second framework. When inferring properties via the first framework, for detected signals with a year-long observation time (which could be higher depending on the detector duty cycle), it is possible to achieve an accuracy of 32% for  $I$  and 16% for  $\alpha$  and  $m_p$ . On the other hand, for inference via the second framework under similar conditions, we observe a comparatively higher accuracy of 1 – 2% or less is achievable for  $I$ ,  $\alpha$ , and  $m_p$ , and 16% accuracy for  $r$ . A key drawback of this framework is that it requires an assumption of a neutron star equation

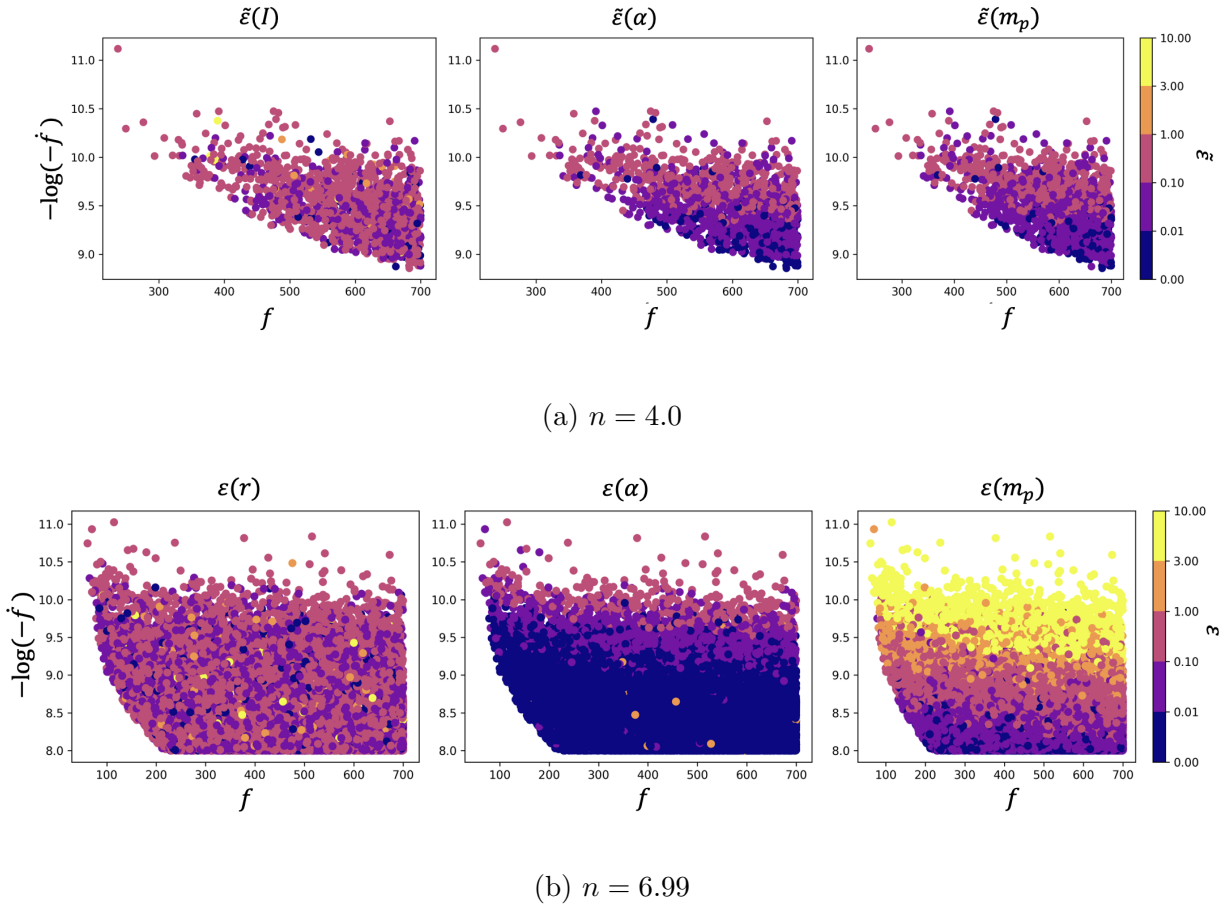


FIG. 8. Inference via framework 2: Relative errors  $\tilde{\epsilon}(I)$ ,  $\tilde{\epsilon}(\alpha)$ ,  $\tilde{\epsilon}(m_p)$ , for braking index  $n = 4, 6.99$ , as function of frequency ( $f$ ) and its derivative ( $\dot{f}$ ). Plotted are median errors for  $T = 1$  year and  $\mathcal{D} = 100 \text{ Hz}^{-1/2}$ . The white areas indicate regions where  $\epsilon > 10$  or  $n_{\text{out}} \notin [3, 7]$  or  $\alpha_s \notin [10^{-6}, 10^{-1}]$ ,  $B < 10^{12} \text{ G}$ , and a total of  $10^5$  points was used.

of state and works only in the slow rotation limit. In contrast, no such requirements are needed for the first framework. The most accurate estimates are when the braking index is in the region  $n \in [4, 6]$ ,  $f$  is small, and  $\dot{f}$  is large.

## B. Assumptions

In this section, we present further discussion on the key assumptions made in our analysis. Firstly, we assume that a supposed CGW detection can be identified as a signal due to r-mode oscillations. It might not be possible if the rotational frequency of the star is not known [22]. In that case, only the value of the braking index ( $n$ ) can give us an idea of

the spin-down mechanism. The CGW signal detected in an all-sky survey could also be due to more exotic sources [23, 24]. However, a successful detection with the gravitational wave frequency ( $f \approx \frac{4}{3}f_{rot}$ ) in targeted/narrow-band searches would strongly imply that the signal is produced by r-modes.

We assume that the spin-down of the star is due to dipolar magnetic field and r-mode oscillations. This leads to a braking index of  $n \in [3, 7]$ , which is inconsistent with current observations [50]. Recent NICER measurements also provide evidence for non-dipolar magnetic fields [51]. Alternative spin-down mechanisms and complex magnetic field models consistent with current observations are still works in progress [52]. Numerous factors other than relativistic effects, such as the magnetic field, influence the r-mode frequency [53]. However, we have ignored these factors due to their negligible effects [28]. Additionally, it's worth noting that r-modes themselves could potentially amplify the magnetic field [54], a consideration which we have chosen to disregard. In this work, we also don't consider stratification, which is shown to be important for realistic mature neutron stars [55].

The universal relations used in the second framework are valid only in a restricted parameter space. The  $\kappa - C$  relation is valid only in the slow-rotation approximation [35] and has corrections of the order of  $(\frac{f}{f_k})^2$  [28], where  $f_k$  is the Kepler frequency. The  $\bar{I} - C$  relation is also not valid for rapidly rotating stars [36] and must be affected by magnetic fields. Similar universal relations called the "I-Love-Q" relation [56], have been shown to become EOS dependent for magnetic fields  $B > 10^{12}\text{G}$  [57]. Although to the best of our knowledge, no similar study exists for  $I - C$  relations used here, such a limit would further restrict the region where the second inference framework can be used. Figure 8 shows the effect of limiting to cases where  $B < 10^{12}\text{G}$ . Only regions close to  $n \approx 7$  have a significant parameter space to estimate. This is mainly because the smaller the magnetic field and the braking index, the smaller the  $\dot{f}$ . As shown in the results, for cases where  $|\dot{f}| < 10^{-11}$ , the condition  $3 < n_{out} < 7$  can not be satisfied.

Kindly note that one could have proceeded with a similar analysis to framework 2 without the  $\bar{I} - C$  relations. As the  $\kappa - C$  relation and an EOS assumption, will give a moment of inertia estimate. In that case, the above-mentioned restriction of parameter space would not be an issue. We opted not to proceed this way as using  $\bar{I} - C$  relations has the potential to infer the moment of inertia directly and thus all the other parameters, without an assumption of EOS (Check VIC).



### C. Mitigating Drawbacks: Potential Solutions.

In this section, we discuss the drawbacks of our work, propose potential solutions to address them and outline future directions for further improvement. The parameter  $\alpha$  ( $\alpha = \alpha_s MR^3 \tilde{J}$ ) is inferred through the first framework. Even if mass and radius measurements become available from electromagnetic observations, there remains an equation of state-dependent parameter  $\tilde{J}$  necessary for estimating the saturation amplitude ( $\alpha_s$ ). It was demonstrated [14] that this parameter is bounded within a factor of 2, suggesting that a fiducial value of  $\tilde{J} \approx 0.01635$  could provide a reasonable rough estimate.

In inference via the second framework, an accurate estimation of all parameters, including the saturation amplitude and distance, can be obtained after assuming an equation of state. It is noteworthy that while the values of the parameters change with the equation of state, the errors remain largely consistent [25]. A prudent approach would involve considering a set of realistic equations of state to calculate potential limits on these parameters.

Low-mass X-ray binaries (LXMBs) represent crucial candidates for signals generated by r-modes [58]. Accurate mass measurements through electromagnetic observations are possible for such systems. Consequently, if we detect a CGW, and such mass measurements exist, one can directly substitute it in the  $I - C$  relation to estimate  $I$ ,  $m_p$ , and  $r$  without assuming any specific equation of state. However,  $\alpha_s$  still necessitates knowledge of  $\tilde{J}$  and the radius of the star, which could also be measured for LXMBs, but possibly not that accurately.

We plan to perform parameter inference by adopting a Bayesian framework in the future, as it would yield robust conclusions and incorporate priors from electromagnetic observations of neutron stars. One could also explore alternate spin-down models encompassing current braking index observations [52] and study more complex magnetic field models rather than a simple dipolar magnetic field to expand on this work [59].

- 
- [1] B. P. Abbott *et al.* (LIGO Scientific, Virgo), *Phys. Rev. Lett.* **116**, 061102 (2016), arXiv:1602.03837 [gr-qc].
  - [2] B. P. Abbott *et al.* (LIGO Scientific, Virgo), *Phys. Rev. X* **9**, 031040 (2019), arXiv:1811.12907 [astro-ph.HE].
  - [3] R. Abbott *et al.* (LIGO Scientific, Virgo), *Phys. Rev. X* **11**, 021053 (2021), arXiv:2010.14527

- [gr-qc].
- [4] B. P. Abbott *et al.* (LIGO Scientific, Virgo), *Astrophys. J. Lett.* **892**, L3 (2020), arXiv:2001.01761 [astro-ph.HE].
- [5] B. P. Abbott *et al.* (LIGO Scientific, Virgo, Fermi GBM, INTEGRAL, IceCube, AstroSat Cadmium Zinc Telluride Imager Team, IPN, Insight-Hxmt, ANTARES, Swift, AGILE Team, 1M2H Team, Dark Energy Camera GW-EM, DES, DLT40, GRAWITA, Fermi-LAT, ATCA, ASKAP, Las Cumbres Observatory Group, OzGrav, DWF (Deeper Wider Faster Program), AST3, CAASTRO, VINROUGE, MASTER, J-GEM, GROWTH, JAGWAR, CaltechNRAO, TTU-NRAO, NuSTAR, Pan-STARRS, MAXI Team, TZAC Consortium, KU, Nordic Optical Telescope, ePESSTO, GROND, Texas Tech University, SALT Group, TOROS, BOOTES, MWA, CALET, IKI-GW Follow-up, H.E.S.S., LOFAR, LWA, HAWC, Pierre Auger, ALMA, Euro VLBI Team, Pi of Sky, Chandra Team at McGill University, DFN, ATLAS Telescopes, High Time Resolution Universe Survey, RIMAS, RATIR, SKA South Africa/MeerKAT), *Astrophys. J. Lett.* **848**, L12 (2017), arXiv:1710.05833 [astro-ph.HE].
- [6] R. Nandi and P. Char, *Astrophys. J.* **857**, 12 (2018), arXiv:1712.08094 [astro-ph.HE].
- [7] R. Nandi, P. Char, and S. Pal, *Phys. Rev. C* **99**, 052802 (2019), arXiv:1809.07108 [astro-ph.HE].
- [8] B. Biswas, P. Char, R. Nandi, and S. Bose, *Phys. Rev. D* **103**, 103015 (2021), arXiv:2008.01582 [astro-ph.HE].
- [9] J. L. Friedman and B. F. Schutz, *Astrophys. J.* **222**, 281 (1978).
- [10] N. Andersson and K. D. Kokkotas, *Int. J. Mod. Phys. D* **10**, 381 (2001), arXiv:gr-qc/0010102.
- [11] B. J. Owen, L. Lindblom, C. Cutler, B. F. Schutz, A. Vecchio, and N. Andersson, *Phys. Rev. D* **58**, 084020 (1998), arXiv:gr-qc/9804044.
- [12] R. Bondarescu, S. A. Teukolsky, and I. Wasserman, *Phys. Rev. D* **76**, 064019 (2007), arXiv:0704.0799 [astro-ph].
- [13] R. Bondarescu, S. A. Teukolsky, and I. Wasserman, *Phys. Rev. D* **79**, 104003 (2009), arXiv:0809.3448 [astro-ph].
- [14] M. G. Alford and K. Schwenzer, *Astrophys. J.* **781**, 26 (2014), arXiv:1210.6091 [gr-qc].
- [15] K. Riles, *Living Rev. Rel.* **26**, 3 (2023), arXiv:2206.06447 [astro-ph.HE].
- [16] B. Steltner, M. Papa, H.-B. Eggenstein, R. Prix, M. Bensch, B. Allen, and B. Machenschalk, *The Astrophysical Journal* **952**, 55 (2023).

- [17] B. P. Abbott *et al.* (LIGO Scientific, VIRGO), *Astrophys. J.* **875**, 122 (2019), [Erratum: *Astrophys. J.* 918, 91 (2021)], arXiv:1812.11656 [astro-ph.HE].
- [18] L. Fesik and M. A. Papa, *The Astrophysical Journal* **895**, 11 (2020).
- [19] B. Rajbhandari, B. J. Owen, S. Caride, and R. Inta, *Physical Review D* **104**, 122008 (2021).
- [20] M. Sieniawska and D. I. Jones, *Mon. Not. Roy. Astron. Soc.* **509**, 5179 (2021), arXiv:2108.11710 [astro-ph.HE].
- [21] N. Lu, K. Wette, S. M. Scott, and A. Melatos, *Mon. Not. Roy. Astron. Soc.* **521**, 2103 (2023), arXiv:2209.10981 [gr-qc].
- [22] D. I. Jones, “Learning from the frequency content of continuous gravitational wave signals,” in *Astrophysics in the XXI Century with Compact Stars* (World Scientific, 2022) Chap. 6, pp. 201–217, arXiv:2111.08561 [astro-ph.HE].
- [23] S. D’Antonio, C. Palomba, P. Astone, S. Frasca, G. Intini, I. La Rosa, P. Leaci, S. Mastroianni, A. Miller, F. Muciaccia, O. J. Piccinni, and A. Singhal, *Phys. Rev. D* **98**, 103017 (2018).
- [24] A. L. Miller, N. Aggarwal, S. Clesse, and F. De Lillo, *Phys. Rev. D* **105**, 062008 (2022), arXiv:2110.06188 [gr-qc].
- [25] S. Ghosh, *Mon. Not. Roy. Astron. Soc.* **525**, 448 (2023), arXiv:2304.12356 [gr-qc].
- [26] P. Jaranowski, A. Królak, and B. F. Schutz, *Phys. Rev. D* **58**, 063001 (1998).
- [27] B. J. Owen, *Phys. Rev. D* **82**, 104002 (2010), arXiv:1006.1994 [gr-qc].
- [28] A. Idrisy, B. J. Owen, and D. I. Jones, *Phys. Rev. D* **91**, 024001 (2015), arXiv:1410.7360 [gr-qc].
- [29] P. Jaranowski and A. Królak, *Phys. Rev. D* **59**, 063003 (1999).
- [30] M. Vallisneri, *Phys. Rev. D* **77**, 042001 (2008).
- [31] R. Prix, *Phys. Rev. D* **75**, 023004 (2007), [Erratum: *Phys. Rev. D* 75, 069901 (2007)], arXiv:gr-qc/0606088.
- [32] C. Dreissigacker, R. Prix, and K. Wette, *Phys. Rev. D* **98**, 084058 (2018).
- [33] B. Behnke, M. A. Papa, and R. Prix, *Phys. Rev. D* **91**, 064007 (2015).
- [34] R. Prix, *Technical Report T0900149-v6, The F-statistic and its implementation in ComputeF-Statistic-v2*, Tech. Rep. (LIGO, 2011).
- [35] S. Ghosh, D. Pathak, and D. Chatterjee, *Astrophys. J.* **944**, 53 (2023), arXiv:2209.11941 [gr-qc].

- [36] C. Breu and L. Rezzolla, *Mon. Not. Roy. Astron. Soc.* **459**, 646 (2016), arXiv:1601.06083 [gr-qc].
- [37] J. H. Taylor and J. M. Cordes, *Astrophys. J.* **411**, 674 (1993).
- [38] R. Smits, S. J. Tingay, N. Wex, M. Kramer, and B. Stappers, *Astron. Astrophys.* **528**, A108 (2011), arXiv:1101.5971 [astro-ph.IM].
- [39] T. Mølnvik and E. Østgaard, *Nucl. Phys. A* **437**, 239 (1985).
- [40] Z. Miao, A. Li, and Z.-G. Dai, *Mon. Not. Roy. Astron. Soc.* **515**, 5071 (2022), arXiv:2107.07979 [astro-ph.HE].
- [41] M. e. a. Kramer, *Phys. Rev. X* **11**, 041050 (2021).
- [42] Abbott, R. and Abbott et. al (LIGO Scientific Collaboration, Virgo Collaboration, and KAGRA Collaboration), *Phys. Rev. D* **104**, 082004 (2021).
- [43] P. Arras, E. E. Flanagan, S. M. Morsink, A. K. Schenk, S. A. Teukolsky, and I. Wasserman, *Astrophys. J.* **591**, 1129 (2003), arXiv:astro-ph/0202345.
- [44] R. Abbott and T. D. e. a. Abbott (LIGO Scientific Collaboration, Virgo Collaboration, and KAGRA Collaboration), *Phys. Rev. D* **105**, 022002 (2022).
- [45] K. Wette, *Astropart. Phys.* **153**, 102880 (2023), arXiv:2305.07106 [gr-qc].
- [46] G. Desvignes *et al.* (EPTA), *Mon. Not. Roy. Astron. Soc.* **458**, 3341 (2016), arXiv:1602.08511 [astro-ph.HE].
- [47] S. K. Dhiman, R. Kumar, and B. K. Agrawal, *Phys. Rev. C* **76**, 045801 (2007).
- [48] R. Nandi and S. Pal, *Eur. Phys. J. ST* **230**, 551 (2021), arXiv:2008.10943 [astro-ph.HE].
- [49] T. Nozawa, N. Stergioulas, E. Gourgoulhon, and Y. Eriguchi, *Astron. Astrophys. Suppl. Ser.* **132**, 431 (1998), arXiv:gr-qc/9804048.
- [50] M. E. Lower *et al.*, *Mon. Not. Roy. Astron. Soc.* **508**, 3251 (2021), arXiv:2109.07612 [astro-ph.HE].
- [51] T. E. Riley *et al.*, *Astrophys. J. Lett.* **918**, L27 (2021), arXiv:2105.06980 [astro-ph.HE].
- [52] A. P. Igoshev and S. B. Popov, *Mon. Not. Roy. Astron. Soc.* **499**, 2826 (2020), arXiv:2008.11737 [astro-ph.HE].
- [53] C. Chirenti and J. Skákala, *Phys. Rev. D* **88**, 104018 (2013), arXiv:1308.3685 [gr-qc].
- [54] J. L. Friedman, L. Lindblom, L. Rezzolla, and A. I. Chugunov, *Physical Review D* **96**, 124008 (2017).
- [55] F. Gittins and N. Andersson, *Mon. Not. Roy. Astron. Soc.* **521**, 3043 (2023), arXiv:2212.04892

[gr-qc].

- [56] K. Yagi and N. Yunes, *Science* **341**, 365 (2013), arXiv:1302.4499 [gr-qc].
- [57] B. Haskell, R. Ciolfi, F. Panarale, and L. Rezzolla, *Mon. Not. Roy. Astron. Soc.* **438**, L71 (2014), arXiv:1309.3885 [astro-ph.SR].
- [58] K. D. Kokkotas and K. Schwenzer, *Eur. Phys. J. A* **52**, 38 (2016), arXiv:1510.07051 [gr-qc].
- [59] A. G. Pili, N. Bucciantini, and L. Del Zanna, *Mon. Not. Roy. Astron. Soc.* **447**, 2821 (2015), arXiv:1412.4036 [astro-ph.HE].